

# Operation of multiphonon-assisted laser in the nanosecond time scales

Huichen Si, Fei Liang,\* Dazhi Lu, Haohai Yu,\* Huaijin Zhang, and Yicheng Wu

Shandong University, State Key Laboratory of Crystal Materials and Institute of Crystal Materials, Jinan, China

**Abstract.** Electron–phonon coupling can tailor electronic transition processes and result in direct lasing far beyond the fluorescence spectrum. The applicable time scales of these kinds of multiphonon-assisted lasers determine their scientific boundaries and further developments, since the response speed of lattice vibrations is much slower than that of electrons. At present, the temporal dynamic behavior of multiphonon-assisted lasers has not yet been explored. Herein, we investigate the Q-switched laser performance of ytterbium-doped  $\text{YCa}_4\text{O}(\text{BO}_3)_3$  (Yb:YCOB) crystal with phonon-assisted emission in nanosecond scales. Using different Q-switchers, the three-phonon-assisted lasers around 1130 nm were realized, and a stable Q-switching was realized in the time domain from submicroseconds to tens of nanoseconds. To the best of our knowledge, this is the longest laser wavelength in all pulse Yb lasers. The minimum pulse width and maximum pulse energy are 29 ns and 204  $\mu\text{J}$ , respectively. These results identify that the electron–phonon coupling is a fast physical process, at least much faster than the present nanosecond pulse width, which supports the operation of multiphonon-assisted lasers in the nanosecond range. In addition, we also provide a simple setup to create pulse lasers at those wavelengths with weak spontaneous emission.

Keywords: pulse lasers; electron–phonon coupling; nanoseconds; Q-switch.

Received Jun. 12, 2023; revised manuscript received Jul. 7, 2023; accepted for publication Jul. 12, 2023; published online Jul. 31, 2023.

© The Authors. Published by SPIE and CLP under a Creative Commons Attribution 4.0 International License. Distribution or reproduction of this work in whole or in part requires full attribution of the original publication, including its DOI.

[DOI: [10.1117/1.APN.2.5.056004](https://doi.org/10.1117/1.APN.2.5.056004)]

## 1 Introduction

Lasers are generated by stimulated radiation during the electronic transition, and since the invention of the laser in 1960,<sup>1</sup> the fluorescence spectra of active materials have become the prerequisite for available laser wavelengths. With the development of gain media, thousands of lasers at the given wavelength from deep ultraviolet to far-infrared have been realized.<sup>2–5</sup> In addition, in the time domain, ultrafast pulse lasers with pulse width from picoseconds to femtoseconds were also developed due to the fast response of electrons.<sup>6</sup> For those laser wavelengths outside the fluorescence spectra of gain media, it is usually not supported by direct lasing but falls back to the nonlinear optical response of electrons, including the second- and high-harmonic generation.<sup>7,8</sup> Nowadays, these lasers are widely employed in various applications, such as laser manufacturing, 3D printing, LASIK surgery, and military confrontation.<sup>9,10</sup>

Laser wavelength extension should be a longtime pursuit for the optical and physics community. Actually, it is possible to obtain laser emission aside spontaneous fluorescence by exploiting the coupling of the electron transitions to lattice vibrations.<sup>11</sup> Recently, our group proposed lasers at the wavelength far beyond the fluorescence spectra of Yb:YCOB with multiphonon-assisted electronic transitions. By controlling the participating phonon numbers, the continuous-wave (CW) lasers at the wavelength of 400 nm beyond the fluorescence envelope were experimentally realized.<sup>12</sup> During the multiphonon-assisted lasing process, the coupling of electron–phonon determines the laser performance, which means that both lattice vibration and electron response should be considered in laser theory. From the view of time domains, the lattice vibration belongs to a slow physical process compared to the electronic response (usually femtosecond scale<sup>13</sup>), since lattice atoms are much heavier than electrons.<sup>14</sup> In general, lattice vibrations have response periods in the picosecond range. The irradiative lifetime of lower energy levels usually ranges from the subnanosecond to milliseconds,<sup>15,16</sup> and the heat transporting

\*Address all correspondence to Fei Liang, [liangfei@sdu.edu.cn](mailto:liangfei@sdu.edu.cn); Haohai Yu, [haohaiyu@sdu.edu.cn](mailto:haohaiyu@sdu.edu.cn)

time scales in the microseconds.<sup>17,18</sup> In theory, the electron–phonon-coupled lasing involves all these physical processes above, and its operation in various time scales should be very interesting. However, in a real material, the intrinsic electronic levels are always overlapped by the electron–phonon-coupled vibronic levels, which results in homogeneously broadened emission. Due to the weak intensity of the electron–phonon coupling effect, the multiphonon-assisted emission usually exhibits an extremely weak cross section, overwhelmed by those pure electronic transitions without phonon participation. Therefore, it is still a great challenge to study the temporal dynamical behavior of multiphonon-assisted lasing beyond the fluorescence spectrum.

Here, associated with the overlapping of the electronic and electron–phonon-coupled vibronic levels and the phonon number dependent transition probability, we demonstrate three-phonon assisted Q-switched Yb:YCOB lasers around 1130 nm with the pulse width covering the nanosecond scales. To the best of our knowledge, this is the longest laser wavelength in all pulse Yb lasers. The minimum pulse width and maximum pulse energy are 29 ns and 204  $\mu\text{J}$ , respectively. These results demonstrate that the electron–phonon coupling is a fast physical process, at least much faster than the present nanosecond pulse width, which supports the operation of multiphonon-assisted lasers in the nanosecond range. In addition, this work opens up new perspectives also for the capacity of ultrafast multiphonon-assisted lasers and paves the way for new frontiers in chirped-pulse amplification and frequency-comb generation.

## 2 Theoretical Analysis for Passive Q-Switch at Fluorescence Sidebands

According to theory of the Q-switched laser,<sup>19</sup> the pulse energy can be expressed as

$$E = \frac{h\nu A}{2\sigma\gamma} \ln\left(\frac{1}{R}\right) \ln\left(\frac{n_i}{n_f}\right), \quad (1)$$

where  $R$  represents the reflectivity of the output coupler,  $h\nu$  represents the photon energy,  $\gamma$  represents inversion reduction factor,  $n_i$  represents the initial inverted population,  $n_f$  represents the residual inverted population,  $A$  represents the laser spot cross sectional area, and  $\sigma$  represents the emission cross section. According to the solution of the rate equations,  $n_i$  and  $n_f$  can be described as

$$n_i = K\tau P_{\text{in}}(1 - e^{-1/f\tau}), \quad (2)$$

$$n_f = n_i e^{-2\sigma n_i (\ln(1/R) + \delta)}, \quad (3)$$

where,  $\tau$  is the fluorescence lifetime,  $P_{\text{in}}$  is the absorbed pump power,  $f$  is the pulse repetition frequency of the Q-switcher,  $\delta$  is the resonator loss factor, and  $K$  is the pumping constant. The gain medium is important in the generation of pulsed lasers. According to Eq. (1), the pulse energy obtained is inversely proportional to the emission cross section of the gain medium.

For ytterbium ion, its electron–phonon intensity is relatively strong owing to a combination of factors from small ionic radius and reduced outer shell  $5s/5p$  orbitals screening.<sup>20</sup> As a result,  $\text{Yb}^{3+}$ -doped laser materials usually exhibit a wide vibronic fluorescence spectrum from 1.0 to  $-1.1 \mu\text{m}$  due to

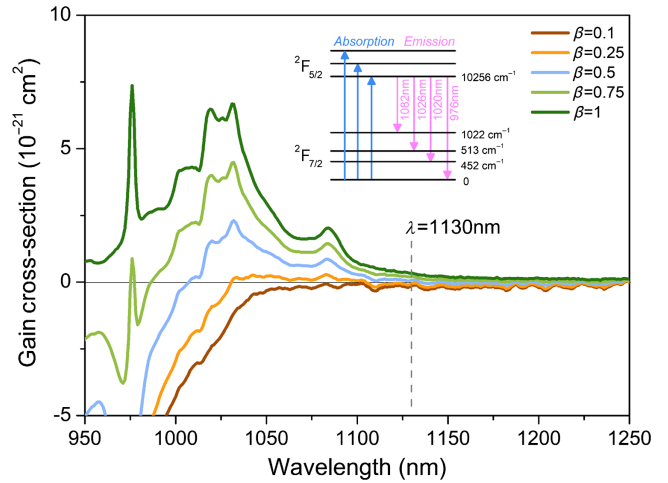


**Fig. 1** Unpolarized gain cross sections of Yb:YCOB crystal. Inset, Stark splitting energy levels of  $\text{Yb}^{3+}$  ion in Yb:YCOB crystal.

homogeneous spectral broadening. Taking the Yb:YCOB crystal as an example, as shown in Fig. 1, at 976, 1020, 1026, and 1082 nm, it has four emission peaks, relating to four Stark splitting lines of  $^2F_{7/2}$  level, respectively. Because of the phonon-assisted vibronic transitions, a long fluorescence sideband beyond 1081 nm appears. The three-phonon-assisted emission cross section at 1130 nm is calculated to be  $3.4 \times 10^{-22} \text{ cm}^2$  from the spectra, which is nearly 1 order of magnitude smaller than that at 1020 and 1082 nm. Such a weak emission usually induces a large laser threshold but is helpful for the energy storage properties when both the lasing and Q-switching thresholds are satisfied.

In addition, considering the pulse width of passive Q-switching, it can be qualitatively expressed as the following equation:

$$\tau = \frac{3.52T_R}{\Delta T}, \quad (4)$$

where,  $T_R$  represents the cavity round-trip time and  $\Delta T$  represents the modulation depth. The present pulse width equation indicates that the modulation depth of the passive Q-switchers should be varied from 0.2% to 20% under the cavity length of about 10 cm with  $T_R = 0.67 \text{ ns}$  for the realization of pulse width ranging from 1  $\mu\text{s}$  to 10 ns. Considering the low absorption of graphene (2.3%) and saturable absorption with normalized modulation depth of about 40%,<sup>21</sup> we can conclude that the graphene could support the Q-switching under the submicrosecond pulse width. For the generation of tens of nanosecond pulse width, we can employ the well-developed Cr:YAG, which has obvious saturable absorption at 1.1  $\mu\text{m}$ . However, the small emission cross section indicates that the loss modulation and initial transmission should be suitable for the balance of laser thresholds and output pulse energy, beside the design of laser cavity.

## 3 Q-Switched Laser Results

### 3.1 Pulsed Laser Operation under Sub-Microsecond Scales with a Monolayer Graphene Modulator

Graphene sheets were pressed onto a far-UV quartz flake as a sample, available as commercial optical grade with a diameter of 5 mm and a thickness of 1 mm. Next, we performed the laser experiments of Yb:YCOB crystal at the fluorescence sidebands.

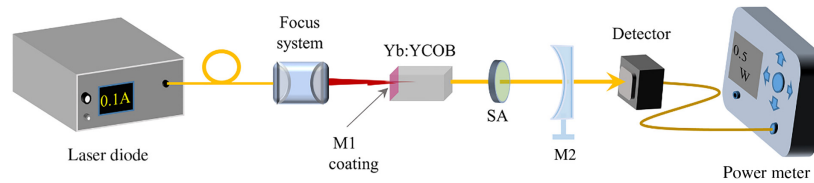


**Fig. 2** Experimental setup for Yb:YCOB laser. SA represents saturable absorber (monolayer graphene and Cr:YAG). M1 is an input mirror directly coated on the front face of the Yb:YCOB crystal.

A compact plano–concave resonator was designed for laser experiment; the schematic illustration is exhibited in Fig. 2. The size of the Yb:YCOB crystal sample with the concentration of 15% (atomic fraction) for laser experiments were  $3\text{ mm} \times 3\text{ mm} \times 6\text{ mm}$ , and Y-cut along its principal optical axis. The absorptivity of crystal to the pump laser is 87% for the single-pass configuration. It was designed for high transmission (HT,  $T > 95\%$ ) from 976 to 1100 nm and high reflection (HR,  $R > 99.9\%$ ) from 1130 to 1200 nm in the front face of the crystal, which served as the input mirror. A plano–concave mirror, M2, as the output mirror, has the curvature radius of 100 mm. It has a certain transmittance ( $T_{oc} = 3\%$ ) in the range of 1130–1200 nm and was also coated for high transmission from 976 to 1100 nm to suppress conventional lasing around 1  $\mu\text{m}$ . Such a compact cavity setup can suppress the pure electronic-transition lasing and improve the laser efficiency at the weak spontaneous emission range. Indium foil-wrapped crystal samples were cooled with circulating water, which was placed in a copper heat sink. Taking into account the heat dissipation during the experiment, a temperature of cooling water was maintained at 20°C. A 30 W fiber-coupled diode laser with a central wavelength of 976 nm was employed as the pump source. The diameter of the fiber core is 105  $\mu\text{m}$  and the numerical aperture (NA) is 0.22. The pump light was focused by the focusing system into the crystal sample at a beam compression ratio of 1:1. For graphene Q-switched vibronic laser, the graphene sample was placed in the laser cavity close to the output

mirror to reduce the possible saturable absorption for pump light and the damage probability of graphene. The laser output power was measured by a power meter (Newport, Model 1916-R), and the pulse repetition rate and pulse width were measured by a TDS-3012 digital oscilloscope (100 MHz bandwidth and 1.25 GS/s sample rate, Tektronix, Inc.). The laser spectrum was recorded by an A.P.E. spectrometer (WaveScan, S/N S09668).

First, we optimized the CW laser at 1130 nm in the Yb:YCOB crystal. Taking into account the thermal lens effect,<sup>22</sup> we can achieve the best pattern-matching by changing the cavity length. Finally, for  $R_{oc} = 100\text{ mm}$ , the laser spot radius in the crystal is about 47  $\mu\text{m}$ . The lasing threshold and the maximum output power are 3.5 and 1.85 W, respectively, with a high slope efficiency of 44.6%, as shown in Fig. 3(a). Figure 3(b) shows the laser spectrum at 1130.9 nm. Notably, we should emphasize that an input mirror, M1, directly coated on the crystal is essential for a stable lasing around 1130 nm. For a separate M1–crystal–M2 setup, we can only obtain 1131 nm lasing under  $T_{oc} = 0.1\%$ , and the laser wavelengths would shift to 1030 nm with higher transmission.

Then, we realized the Q-switched pulse laser operation by inserting a graphene modulator. The Q-switched laser wavelength is 1130.4 nm, which is slightly blueshifted compared to the CW laser, as shown in Fig. 3(b). This wavelength shift can be attributed to the reflection loss caused by the uncoated quartz substrates. Figure 3(a) displays the output powers of the Q-switched laser. It is observed that the lasing threshold

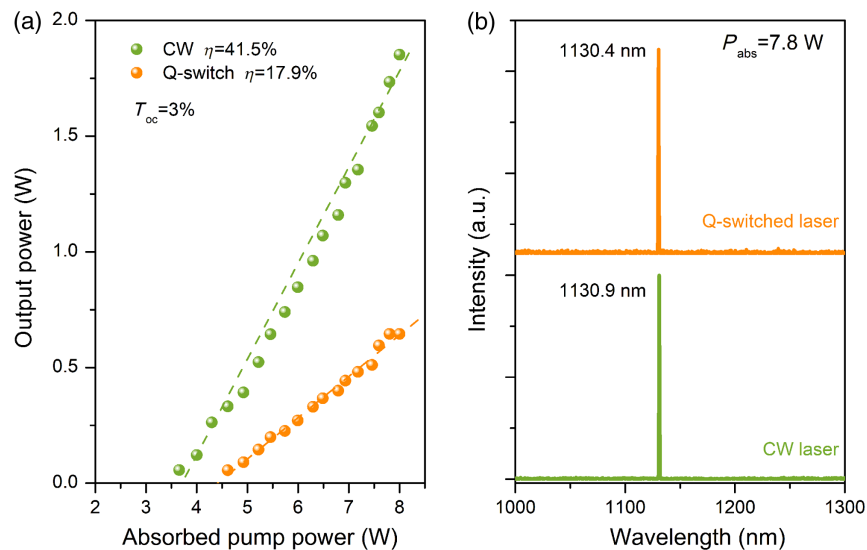


**Fig. 3** Graphene Q-switch pulse laser generation of Yb:YCOB crystal at 1130 nm. (a) Output powers of the Yb:YCOB crystal under CW and Q-switched regimes. The dashed lines represent the fitting curves.  $\eta$  is the slope efficiency. (b) Lasing wavelength under CW and Q-switched regimes.

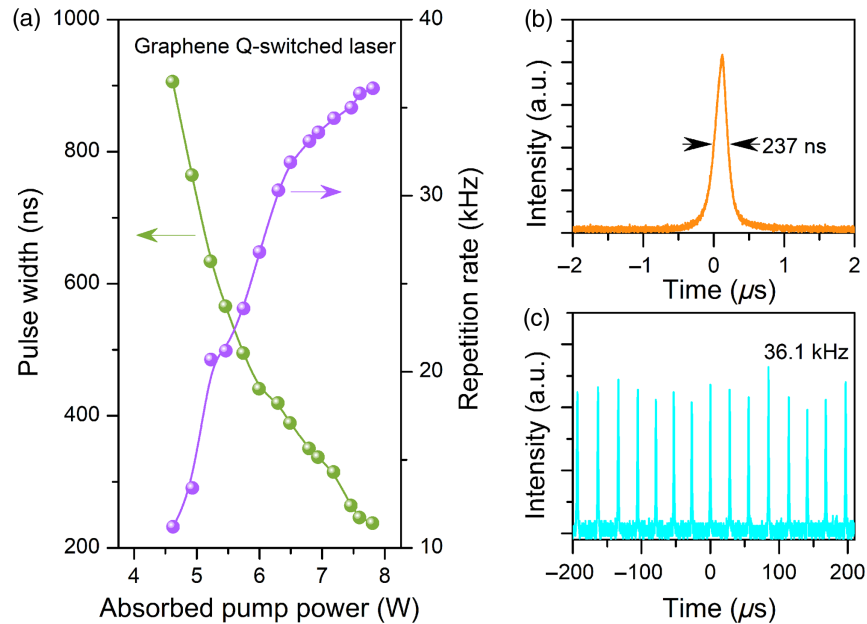


**Fig. 4** Graphene Q-switched pulse laser properties. (a) Pulse width and repetition under different pump powers. (b) Corresponding individual pulse profiles. (c) Laser pulse trains with reception of 36.1 kHz.

increases and slope efficiency decreases after inserting the graphene sample, owing to an external optical loss of passive Q-switches. The Q-switched lasing threshold is 4.45 W. And the slope efficiency is 17.9%, with a maximum average pulse laser output power of 645 mW.

The variations of Q-switched pulse width and repetition rate under different pump powers are displayed in Fig. 4(a). With increasing absorbed pump power, it shows a typical characteristic for passive Q-switched laser that the pulse repetition rate increases from 11.2 to 36.1 kHz, and the pulse width decreases from 0.9  $\mu\text{s}$  to 237 ns. As shown in Figs. 4(b) and 4(c), when the absorbed pump increases to 7.8 W, the pulse width reduces to 237 ns. At this time, the corresponding repetition rate is 36.1 kHz, and the amplitude fluctuations in the pulse train are 27%. In addition, we can see that the pulse width of this vibronic laser at 1130 nm is comparable to that of conventional lasing around 1  $\mu\text{m}$  in Yb-doped laser materials using the same graphene saturable absorber (SA),<sup>23</sup> but the pulse repetition rate is much smaller. Obviously, the pulses are completed and no satellite pulses or modulations in the pulse profile are observed, which indicates that the electron–phonon coupling is fast enough compared with the submicrosecond scales.

Moreover, pulse energy and peak power are two important factors for a Q-switched solid-state laser, especially for some special cases with a demand for high-power applications. Based on the experimental results, we calculated the pulse energy and peak power by combining the repetition rate, pulse width, and average output power, as shown in Fig. 5. The pulse energy and peak power gradually become larger and larger as absorbed pump power increases. The maximum single pulse energy is 17.9  $\mu\text{J}$ . The peak power is calculated to be 75 W. According to the configuration in the Q-switching experiments, the laser spot radius in the graphene sample is around 232.8  $\mu\text{m}$ . The intracavity intensity on the SA reaches 1.4  $\text{MW}/\text{cm}^2$ , which is much smaller than the saturation intensity of the monolayer graphene (MLG) sample ( $I_s = 1.5 \text{ GW}/\text{cm}^2$  at 1100 nm).<sup>24</sup>

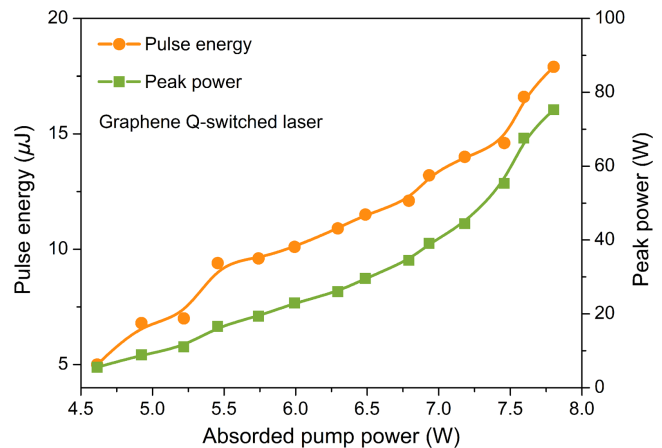


**Fig. 5** Change of pulse energy and peak power with absorbed pump power.

### 3.2 Pulsed Laser Operation under Tens of Nanosecond Scales with a Cr:YAG Modulator

For the generation of tens of nanosecond pulse width, we can employ the well-developed Cr:YAG, which has obvious saturable absorption at 1.1  $\mu\text{m}$ . For the balance of thresholds of lasers and Q-switching and pulse width, a Cr:YAG plate with the optimized initial transmission of  $T_0 = 97\%$  and AR coating from 1120 to 1150 nm, was employed in the Q-switching. In order to reduce the insertion loss and improve bleaching rate, Cr:YAG was placed slightly closer to the laser crystal to ensure a small incident laser beam size and reduce the threshold of the Q-switched laser. Two output couplers with  $T_{oc} = 0.1\%$  and 1% were utilized. For CW laser, as shown in Fig. 6(a), the lasing threshold is about 3.1 W. Meanwhile, the efficiency and output power are improved by increasing output mirror transmittance.

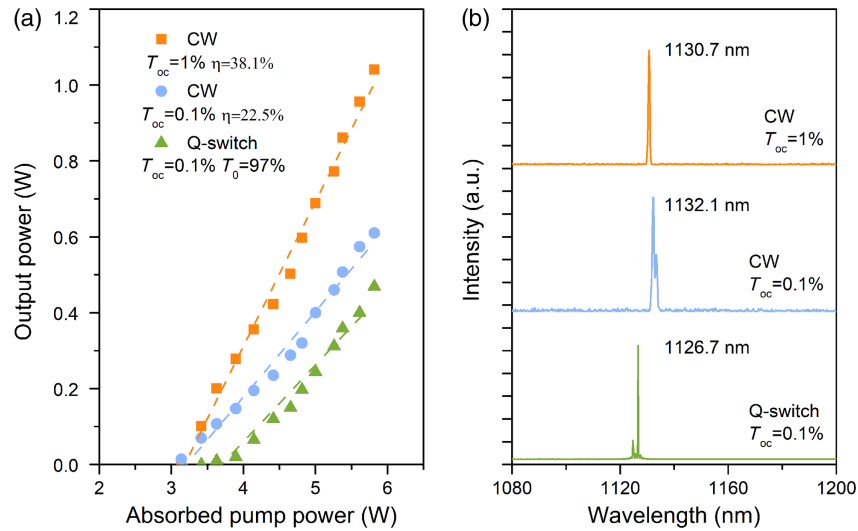


**Fig. 6** Cr:YAG Q-switch pulse laser generation of Yb:YCOB crystal at 1130 nm. (a) Output powers of the Yb:YCOB crystal under CW and Q-switched regime. The solid lines represent the fitting curves.  $\eta$  is the slope efficiency. (b) Lasing wavelengths under CW and Q-switched regime.

The slope efficiency for  $T_{oc} = 0.1\%$  is 22.5% with 610 mW output power. In comparison, the highest power reaches up to 1.04 W for  $T_{oc} = 1\%$  with a high slope efficiency of 38.1%. The laser wavelengths for  $T_{oc} = 0.1\%$  and 1% are 1132.1 and 1130.7 nm, respectively, as shown in Fig. 6(b).

For  $T = 0.1\%$ , a Q-switched pulse laser output was realized by inserting a Cr:YAG plate. The maximum average output power reached 469 mW when the absorbed pump power was 5.8 W. The slope efficiency decreased to 20.2% and the lasing threshold increased to 3.65 W, owing to external in-cavity loss of Cr:YAG. Meanwhile, the central wavelength of the Q-switched laser was blueshifted to 1126.7 nm. We also tried the Q-switched pulse laser with  $T_{oc} = 1\%$ . However, under this

high transmittance, we did not achieve pulsed laser operation when inserting a Cr:YAG switch. This case can be explained from the coupled rate equations of a pulse laser. Due to the small emission cross section at 1130 nm, the value of the initial transmission ( $T_0$ ) and the reflectivity for the output mirror ( $R$ ) must be large enough to yield a moderate population density and reduce pulse laser threshold. In our experiments, when  $T_{oc}$  increased from 0.1% to 1%, the reduced reflectivity would break this condition. Therefore, low-gain medium needs to be characterized by higher optimum mirror reflectivity for a passively Q-switched pulse laser.

Figure 7 shows the variation of the repetition rate frequency (PRF) and pulse width as a function of the absorbed pump

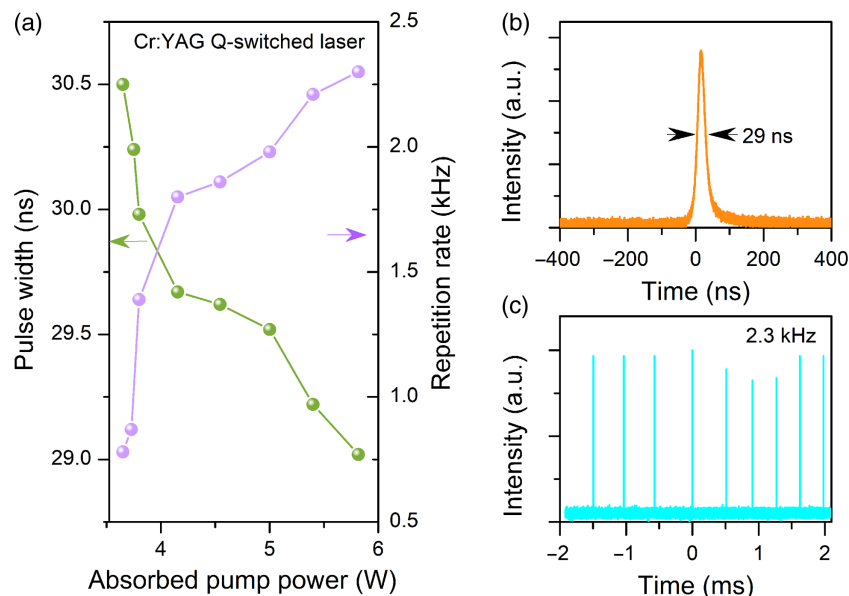


**Fig. 7** (a) Pulse width and repetition under different pump powers. (b) Corresponding individual pulse profiles. (c) Laser pulse trains with reception of 2.3 kHz.

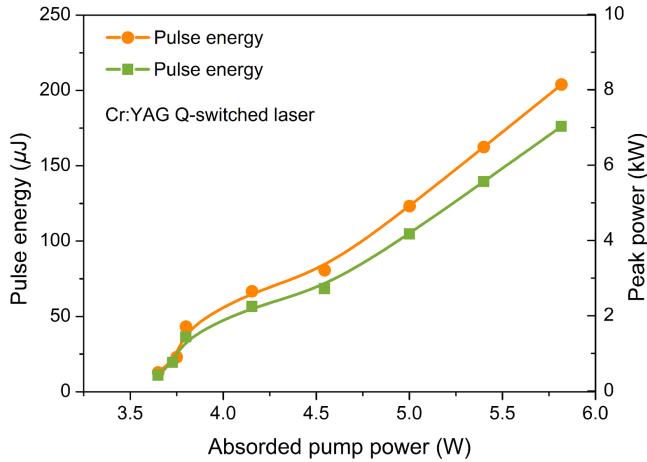


**Fig. 8** Change of pulse energy and peak power with absorbed pump power.

power recorded by the oscilloscope. As shown in Fig. 7(a), as the absorption pump power increases, PRF increases from 0.78 to 2.3 kHz, and the pulse width decreases from 30.5 to 29 ns, which is a typical feature of passively Q-switched lasers. When the absorbed pump power increases to 5.82 W, Fig. 7(b) shows the shortest pulse width, 29 ns. At this time, the corresponding PRF is 2.3 kHz. A uniform and stable pulse train is shown in Fig. 7(c). From this figure, it can be found that the pulses are also smooth and there are no satellite pulses or modulations in the pulse profile, which indicates that the electron–phonon coupling is fast enough for pulse laser operation. In 1981, Wiesenfeld and Mollenauer reported that the configurational relaxation time of KCl:Li crystal is on the tens of picosecond scale,<sup>25</sup> which is consistent with our conclusion.

For 1126 nm lasing in the Yb:YCOB crystal, the pulse energy and peak power as a function of the absorbed pump power

are shown in Fig. 8. It is observed that with the increasing absorbed pump power, both pulse energy and peak power gradually increase. This trend is also similar to that in the Yb:YCOB laser around 1030 and 1080 nm.<sup>26,27</sup> The maximum energy of single pulse and peak power are 204 μJ and 7.03 kW, respectively.

Finally, we make a comprehensive comparison for solid-state Q-switched lasers of the Yb:YCOB series crystal. As listed in Table 1, all laser wavelengths of the Yb:YCOB crystal locate around 1020, 1030, and 1080 nm, corresponding to its strong emission peaks on the fluorescence spectrum. In this work, we realized the first Q-switched Yb:YCOB laser beyond 1.1 μm with a short pulse width and high pulse energy. For most Yb<sup>3+</sup> ions lasers operating on the  $^2F_{5/2} \rightarrow ^2F_{7/2}$  transition, the laser is emitted in a range of 1000–1100 nm. To the best of our knowledge, this Q-switched lasing around 1130 nm is also the longest wavelength among all Yb-doped laser materials, including fibers, ceramics, and crystals. Therefore, it represents a great breakthrough for laser physical and laser engineering. These experimental results show that it is feasible to achieve high-energy laser pulses at the fluorescence sidebands, even better than traditional lasing inside the fluorescence spectrum. In addition, it is worth pointing out that this vibronic Q-switched pulse laser differs from previous spectral satellite peaks beyond 1100 nm in ultrafast Yb-lasers,<sup>38–40</sup> from which the Raman scattering effect mainly dominates the position and intensity of satellites. Our laser at 1130 nm is a direct vibronic lasing by amplifying the phonon-assisted emission at the fluorescence sidebands.<sup>12,41</sup> There is no concurrent lasing at the strong fluorescence peaks of the Yb:YCOB crystal.

## 4 Conclusion

Based on multiphonon coupling strategy, we studied the pulsed laser operation of three-phonon-assisted pulsed Yb:YCOB lasers in the nanosecond time scales from 0.9 ns to 29 ns. By optimizing the cavity, we identified that the electron–phonon

**Table 1** Laser activities of Q-switched Yb:YCOB and Yb:GdCOB laser.<sup>a</sup>

Q-switch	$\lambda_p$ (nm)	$P_{avr}$ (W)	PRF (kHz)	$T_p$ (ns)	$E_p$ (μJ)	$P_p$ (kW)
AO <sup>28</sup>	1027.5	0.95	0.2	11	4750	432
AO <sup>29</sup>	1020 and 1023	0.53	0.1	21	5300	252.4
SA: Cr:YAG <sup>30</sup>	1030 to 1035	2.14	4.5	9.3	476	51.2
SA: Cr:YAG <sup>31</sup>	1031.5	4.2	5.7	3.6	737	205
SA: Cr:YAG <sup>32</sup>	1022 and 1031.8	4.13	3.23	5	1280	256
SA: MoTe <sub>2</sub> <sup>33</sup>	1035.5	1.58	704	52	2.25	0.04
SA: WS <sub>2</sub> <sup>34</sup>	1033.5 and 1036.4	4.05	606	66	6.67	0.1
SA: Bi <sub>2</sub> Te <sub>3</sub> <sup>35</sup>	1030.3 and 1033.3	3.85	400	96	9.63	0.1
SA: GaAs <sup>36</sup>	1032	5.7	116.7	153	48.8	0.32
SA: GaAs <sup>37</sup>	1022.7	1.02	1	13.6	1020	75
SA: InGaAs QWs <sup>27</sup>	1086	1.15	7	100	165	1.65
SA: graphene (this work)	1130.4	0.645	36.1	237	17.9	0.075
SA: Cr:YAG (this work)	1126.7	0.469	2.3	29	204	7.03

<sup>a</sup>AO, acousto-optic; SA, saturable absorber; QWs, quantum wells;  $\lambda_p$ , central wavelength of the pulse laser;  $P_{avr}$ , average power of the pulse laser; PRF, repetition rate;  $T_p$ , pulse width;  $E_p$ , pulse energy;  $P_p$ , peak power of the pulse laser.

coupling is a fast enough physical process compared with the nanosecond scales. We believe that this work should be helpful for the understanding of the electron–phonon coupling effect during the lasing process in the time view. This work provides a kind of pulsed lasers at rare wavelengths representing the longest wavelength among all Yb<sup>3+</sup>-based Q-switched pulse lasers. According to our previous CW laser results, higher-order phonon-assisted Q-switched pulse lasers can be expected at the longer wavelengths. Moreover, this work provides a reliable method for the realization of extended laser wavelengths in the pulse regime and should be feasible in other laser materials, such as Nd<sup>3+</sup>, Tm<sup>3+</sup>, and Er<sup>3+</sup>-doped laser materials. Considering the broad, flat, and smooth gain profiles of multiphonon-assisted fluorescence sidebands, it is also possible to realize an ultrafast mode-locked laser operation at these long wavelengths and consequently extend the potential laser applications in many scientific fields.

### Code, Data, and Materials Availability

The data that support the findings of this article are not publicly available due to privacy. They can be requested from the author at liangfei@sdu.edu.cn.

### Acknowledgments

This work was supported by the National Key Research and Development Program of China (Grant Nos. 2021YFA0717800 and 2021YFB3601504), the National Natural Science Foundation of China (Grant Nos. 52025021, 51890863, and 52002220), and the Future Plans of Young Scholars at Shandong University.

### References

1. T. H. Maiman, “Stimulated optical radiation in ruby,” *Nature* **187**, 493–494 (1960).
2. C. Krankel et al., “Out of the blue: semiconductor laser pumped visible rare-earth doped lasers,” *Laser Photonics Rev.* **10**, 548–568 (2016).
3. A. Richter et al., “Continuous-wave ultraviolet generation at 320 nm by intracavity frequency doubling of red-emitting praseodymium lasers,” *Opt. Express* **14**, 3282–3287 (2006).
4. J. Zou et al., “3.6 W compact all-fiber Pr<sup>3+</sup>-doped green laser at 521 nm,” *Adv. Photonics* **4**, 056001 (2022).
5. T. J. Carrig and A. M. Schober, “Mid-infrared lasers,” *IEEE Photonics J.* **2**, 207–212 (2010).
6. A. Penzkofer, “Passive Q-switching and mode-locking for the generation of nanosecond to femtosecond pulses,” *Appl. Phys. B-Photophys. Laser Chem.* **46**, 43–60 (1988).
7. H. Mao et al., “Noncritical quasiphase-matched second harmonic generation in LiB<sub>3</sub>O<sub>5</sub> crystal at room temperature,” *Appl. Phys. Lett.* **61**, 1148–1150 (1992).
8. S. Zhu, Y. Y. Zhu, and N. B. Ming, “Quasi-phase-matched third-harmonic generation in a quasi-periodic optical superlattice,” *Science* **278**, 843–846 (1997).
9. S. Wang et al., “High efficiency nanosecond passively Q-switched 2.3 μm Tm:YLF laser using a ReSe<sub>2</sub>-based saturable output coupler,” *OSA Contin.* **2**, 1676–1682 (2019).
10. T. Y. Fan and R. L. Byer, “Diode laser-pumped solid-state lasers,” *IEEE J. Quantum Electron.* **24**, 895–912 (1988).
11. L. F. Johnson, R. E. Dietz, and H. J. Guggenheim, “Optical maser oscillation from Ni<sup>2+</sup> in MgF<sub>2</sub> involving simultaneous emission of phonons,” *Phys. Rev. Lett.* **11**, 318–320 (1963).
12. F. Liang et al., “Multiphonon-assisted lasing beyond the fluorescence spectrum,” *Nat. Phys.* **18**, 1312–1316 (2022).
13. S. Smolorz and F. Wise, “Femtosecond two-beam coupling energy transfer from Raman and electronic nonlinearities,” *J. Opt. Soc. Am. B* **17**, 1636–1644 (2000).
14. G. Blasse, “Vibronic transitions in rare earth spectroscopy,” *Int. Rev. Phys. Chem.* **11**, 71–100 (1992).
15. Y. B. Chung, I. W. Lee, and D. J. Jang, “Ultrafast lattice vibrational-relaxation of optically-excited f-centers in RBCL at 4.2 K,” *Opt. Commun.* **86**, 41–44 (1991).
16. D. B. Straus et al., “Direct observation of electron-phonon coupling and slow vibrational relaxation in organic-inorganic hybrid perovskites,” *J. Am. Chem. Soc.* **138**, 13798–13801 (2016).
17. D. Y. Tzou and J. K. Chen, “Thermal lagging in random media,” *J. Thermophys. Heat Transf.* **12**, 567–574 (1998).
18. A. H. Atabaki et al., “Optimization of metallic microheaters for high-speed reconfigurable silicon photonics,” *Opt. Express* **18**, 18312–18323 (2010).
19. S. Ma et al., “High repetition rates optically active langasite electro-optically Q-switched laser at 1.34 μm,” *Opt. Express* **25**, 24007–24014 (2017).
20. A. Ellens et al., “Spectral-line-broadening study of the trivalent lanthanide-ion series. II. The variation of the electron-phonon coupling strength through the series,” *Phys. Rev. B* **55**, 180–186 (1997).
21. J. Wang et al., “Broadband nonlinear optical response of graphene dispersions,” *Adv. Mater.* **21**, 2430–2435 (2009).
22. S. Chenais et al., “Thermal lensing measurements in diode-pumped Yb-doped GdCOB, YCOB, YSO, YAG and KGW,” *Opt. Mater.* **22**, 129–137 (2003).
23. J. M. Serres et al., “Q-switching of Yb:YGG, Yb:LuGG and Yb:CNGG lasers by a graphene saturable absorber,” *Opt. Quantum Electron.* **48**, 197 (2016).
24. H. Z. Yang, Q. Wang, and W. Ji, “Laser-pulse-duration and spectral dependence of saturable absorption in graphene,” *Proc. SPIE* **8205**, 82050J (2011).
25. J. M. Wiesenfeld, L. F. Mollenauer, and E. P. Ippen, “Ultrafast configurational relaxation of optically excited color centers,” *Phys. Rev. Lett.* **47**, 1668–1671 (1981).
26. J. H. Liu et al., “Continuous-wave and passive Q-switching laser performance of Yb:YCa<sub>4</sub>O(BO<sub>3</sub>)<sub>3</sub> crystal,” *IEEE J. Sel. Top. Quantum Electron.* **21**, 348–355 (2015).
27. H. C. Liang et al., “Passively Q-switched Yb<sup>3+</sup>:YCa<sub>4</sub>O(BO<sub>3</sub>)<sub>3</sub> laser with InGaAs quantum wells as saturable absorbers,” *Appl. Opt.* **46**, 2292–2296 (2007).
28. X. Chen et al., “Acousto-optic Q-switching laser performance of Yb:GdCa<sub>4</sub>O(BO<sub>3</sub>)<sub>3</sub> crystal,” *Appl. Opt.* **54**, 7142–7147 (2015).
29. X. Chen et al., “Compact repetitively Q-switched Yb:YCa<sub>4</sub>O(BO<sub>3</sub>)<sub>3</sub> laser with an acousto-optic modulator,” *Opt. Laser Technol.* **70**, 128–130 (2015).
30. J. Liu et al., “The potential of Yb:YCa<sub>4</sub>O(BO<sub>3</sub>)<sub>3</sub> crystal in generating high-energy laser pulses,” *Opt. Express* **21**, 9365–9376 (2013).
31. X. Chen et al., “High-power CW and passively Q-switched laser operation of Yb:GdCa<sub>4</sub>O(BO<sub>3</sub>)<sub>3</sub> crystal,” *Opt. Laser Technol.* **79**, 74–78 (2016).
32. J. Liu et al., “Continuous-wave and passive Q-switching laser performance of Yb:YCa<sub>4</sub>O(BO<sub>3</sub>)<sub>3</sub> crystal,” *IEEE J. Sel. Top. Quantum Electron.* **21**, 1600808 (2015).
33. Y. Ma et al., “Passive Q-switching induced by few-layer MoTe<sub>2</sub> in an Yb:YCOB microchip laser,” *Opt. Express* **26**, 25147–25155 (2018).
34. K. Tian et al., “High-power Yb:YCa<sub>4</sub>O(BO<sub>3</sub>)<sub>3</sub> laser passively Q-switched by a few-layer WS<sub>2</sub> saturable absorber,” *Opt. Laser Technol.* **113**, 1–5 (2019).
35. J. Yang et al., “High-power passive Q-switching performance of a Yb:YCa<sub>4</sub>O(BO<sub>3</sub>)<sub>3</sub> laser with a few-layer Bi<sub>2</sub>Te<sub>3</sub> topological insulator as a saturable absorber,” *Opt. Mater. Express* **8**, 3146–3154 (2018).

36. X. Chen et al., “High-power passively Q-switched Yb:YCa<sub>4</sub>O(BO<sub>3</sub>)<sub>3</sub> laser with a GaAs crystal plate as saturable absorber,” *Appl. Opt.* **54**, 3225–3230 (2015).
37. J. Liu et al., “Passively Q-switched Yb:YCa<sub>4</sub>O(BO<sub>3</sub>)<sub>3</sub>/GaAs laser generating 1 mJ of pulse energy,” *IEEE Photonics Technol. Lett.* **28**, 1104–1106 (2016).
38. A. Yoshida et al., “Diode-pumped mode-locked Yb:YCOB laser generating 35 fs pulses,” *Opt. Lett.* **36**, 4425–4427 (2011).
39. S. Kimura, S. Tani, and Y. Kobayashi, “Raman-assisted broadband mode-locked laser,” *Sci. Rep.* **9**, 3738 (2019).
40. P. Loiko et al., “Multiphonon-assisted emission of rare-earth ions: towards pulse shortening in mode-locked lasers,” in *Laser Congr. 2022 (ASSL, LAC, LS&C)*, Optica Publishing, p. AM2A.2 (2022).
41. P. Loiko et al., “Highly-efficient 2.3 μm thulium lasers based on a high-phonon-energy crystal: evidence of vibronic-assisted emissions,” *J. Opt. Soc. Am. B* **38**, 482–495 (2021).

Biographies of the authors are not available.